Removal of Cl- from WFGD Wastewater by Electrocoagulation using Layered Double Hydroxide Compounds as Granule Electrodes

Xiang Li[1], Wen-Yi Tan[2,], Jian-Gang Lu[1,*], Hai-Yun Zhang[2], Hang Li[2], Chen Zhou[3], Jian-Wei Chen[3]*

[1] Jiangsu Collaborative Innovation Center of Atmospheric Environment and Equipment Technology, Jiangsu Key Laboratory of Atmospheric Environment Monitoring and Pollution Control, Nanjing University of Information Science and Technology, Nanjing 210044, P R China
[2] Department of Environment Engineering, Nanjing Institute of Technology, Nanjing 211167, P R China
[3] China Power Hua Chuang Electricity Technology Research Co., Ltd, 200086, Shanghai, P R China
*E-mail: twy1102@gmail.com; jglu@nuist.edu.cn

Wet flue gas desulfurization (WFGD) wastewater contains a considerable amount of Cl-, which can cause equipment and pipeline corrosion and even reduce desulfurization efficiency. An electrocoagulation (EC) process with three-dimensional electrodes, consisting of layered double hydroxide (LDH) compounds as granule electrodes and Fe as plate electrodes, was adopted to remove Cl- from WFGD wastewater. Two kinds of layered double hydroxide compounds, ZnAl-NO$_3$ layered double hydroxides (LDHs) and MgAl-CO$_3$ calcined layered double hydroxides (CLDHs), were comparatively investigated as granule electrodes and coupled with an EC process. The feasibility and effectiveness of layered double hydroxides as granule electrodes for Cl- removal were proven by X-ray diffraction (XRD) and Fourier transform infrared (FTIR) characterization. The morphology and thermal stability of the layered double hydroxides were further demonstrated by means of scanning electron microscopy (SEM) and thermogravimetry (TG). When ZnAl-NO$_3$ LDHs were used as the granule electrode, the removal efficiency of Cl- reached 84.19% at an electrode spacing of 1 cm, a current density of 444 A/m^2, and an electrolysis time of 20 min. When a MgAl-CO$_3$ CLDH granule electrode was used, the removal efficiency of Cl- reached 83.78% under an electrode spacing of 1 cm, a current density of 333 A/m^2 and an electrolysis time of 20 min. Cl- removal was enhanced by the coupling of the EC process with adsorption by layered double hydroxide compounds.

1. INTRODUCTION

By the end of 2017, the total capacity of coal-fired power plants equipped with flue gas desulfurization (FGD) units was 123,578 MW [1] in China. The limestone-gypsum wet flue gas

desulfurization (WFGD) process has high desulfurization efficiency and low operation cost [2,3]. This technology is widely applied in coal-fired power plants in China. However, a certain amount of wastewater with an extremely complex composition must be discharged regularly from the WFGD process. In general, desulfurization wastewater mainly contains a large amount of soluble salts (especially Cl-), suspended solids and trace heavy metals [4]. High concentrations of Cl- are difficult to address in desulfurization wastewater for most coal-fired power plants [5], which leads to many negative effects. Such effects include the corrosion of rendering equipment and pipelines and even indirect effects on the desulfurization efficiency [6]. Therefore, WFGD wastewater must be discharged with adequate treatment. To date, many Cl- removal technologies have been applied in desulfurization wastewater treatment systems, such as chemical precipitation, evaporation crystallization, electrodialysis, and reverse osmosis (RO). However, there are many problems with these methods. In most domestic coal-fired power plants, the chemical precipitation method cannot easily remove the high concentration of Cl- in WFGD wastewater [4]. The operation and maintenance costs of evaporative crystallization and electrolysis-electrodialysis processes are too high [7,8]. Membrane fouling in RO leads to higher operating pressure and reduces membrane life [9].

In recent years. EC has become an attractive method for industrial wastewater treatment and has been applied in WFGD wastewater treatment abroad [10]. Our group adopted EC technology to treat desulfurization wastewater, and the effects of initial pH, electrolysis time, cell voltage and electrode spacing on the removal of turbidity and heavy metals were studied [11]. For the EC process, there is no need to add chemical reagents, and therefore, no secondary pollution risk happens. Moreover, EC can be coupled with other technologies to form an advantageous combined process with more economical and reasonable properties for purifying wastewater [12].

Layered double hydroxides (LDHs) are promising anion adsorption materials for wastewater treatment on the industrial scale [13]. The structure of a typical LDH can be expressed by the following formula:

$$[M^{2+}_{1-x}M^{3+}_x \times OH_2]^{x+}(A^{n-})_{x/n} \cdot mH_2O$$
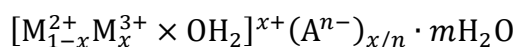
M^{2+} and M^{3+} are divalent and trivalent metal cations; x is the $M^{3+}/(M^{2+}+M^{3+})$ molar ratio and generally has a value ranging from 0.2 to 0.3; and A^{n-} is the charge-balancing inorganic or organic anion [14-16]. LDHs and their calcined products have been used as adsorbents to treat wastewater containing Cl-, such as chloride-rich simulated concrete pore solution [17], sodium carbonate manufacturing wastewater [18] and landfill wastewater [19]. Yang et al. used modified Ca-Al NO$_3$ LDH to treat Cl- in simulated concrete pore solution [17]. Roya Hamidi et al. utilized Mg-Al LDH synthesized by the precipitation method for the simultaneous removal of Mg^{2+}, Ca^{2+} and Cl- from sodium carbonate manufacturing wastewater, and the removal efficiency of Ca^{2+} and Cl- was greater than 90% [18]. Tomohito Kameda et al. observed that the removal efficiency of Cl- in landfills reached 90% when calcined hydrotalcite (Mg–Al oxide) was used [19].

In this study, ZnAl-NO$_3$ LDHs and MgAl-CO$_3$ CLDHs synthesized by a coprecipitation-hydrothermal method were introduced for the first time into a traditional two-dimensional electrocoagulation reactor. Thus, a three-dimensional electrode system was constructed for Cl- removal in desulfurization wastewater, and the adsorption merits of LDH/CLDH were integrated with electrochemical technology. To the best of our knowledge, few studies have reported this novel

technology. The addition of CLDH as a granule electrode improved the Cl⁻ removal performance. The chlorine loading effect of the granule electrodes was verified by XRD and FTIR characterization.

2. EXPERIMENTAL

2.1. Materials and preparation

The ZnAl-NO₃ LDHs, MgAl-CO₃ LDHs and MgAl-CO₃ CLDHs were synthesized by using a coprecipitation-hydrothermal method. $Mg(NO_3)_2 \cdot 6H_2O$ and $Al(NO_3)_3 \cdot 9H_2O$ with a M^{2+}/Al^{3+} molar ratio of 2.0 were dissolved in decarbonated water in a 500 mL flask (M=Mg or Zn); a 0.2 M concentration of the desired anion (NO_3^- or CO_3^{2-}) and 2 M NaOH were simultaneously dripped into the nitrate mixed solution with stirring under a nitrogen atmosphere. The synthesis of MgAl-CO₃ LDHs does not require a N_2 atmosphere. The final pH of the mixture was maintained at approximately 9.0 for ZnAl-NO₃ LDHs and 10.0 for MgAl-CO₃ LDHs. The resulting slurry was hydrothermally treated at 70°C for 24 h to improve its crystallinity. Then, the products were dried at 100°C for 24 h and ground to obtain ZnAl-NO₃ LDHs and MgAl-CO₃ LDHs. The prepared MgAl-CO₃ LDHs were finally calcined at 500°C for 3 h in a muffle furnace, and MgAl-CO₃ CLDHs were obtained.

2.2. Characterization

The crystal structures of the materials were analyzed by XRD using an XD-3 diffractometer (Beijing Puhua General Instrument Co., Ltd.) with Cu Kα (λ=1.5406 Å) radiation (36 kV and 30 mA) at a scanning rate of 5 min⁻¹. The LDH samples were used to prepare KBr pellets, and FTIR spectra in the range of 4000–650 cm⁻¹ were recorded with an MB154S FTIR infrared spectrometer (Bomen, Canada). TG and DSC analyses of the LDH samples were performed under a nitrogen atmosphere using an SDTQ600 TA (US) at a heating rate of 10°C/min in the temperature range of 30-700°C. SEM analyses were performed on a LVXJSM6360 scanning microscope at an accelerating voltage of 5 kV.

Postsorption characterization: A 200 mL volume of wastewater was mixed with ZnAl-NO₃ LDHs (e.g., 0.4 g) at a stirring rate of 300 rpm for 6 h under a nitrogen atmosphere. After reaching equilibrium, the residual solid was characterized by XRD and FTIR. Correspondingly, MgAl-CO₃ CLDHs were characterized by a similar procedure to that used for ZnAl-NO₃ LDHs.

2.3. Apparatus

The EC reactor was composed of a 1.6 L liquid reaction cell, and two parallel Fe plates (20×4.5 cm²) were immersed vertically into wastewater with an electrode spacing of 1-3 cm. Fig. 1 shows the three-dimensional electrocoagulation reactor.
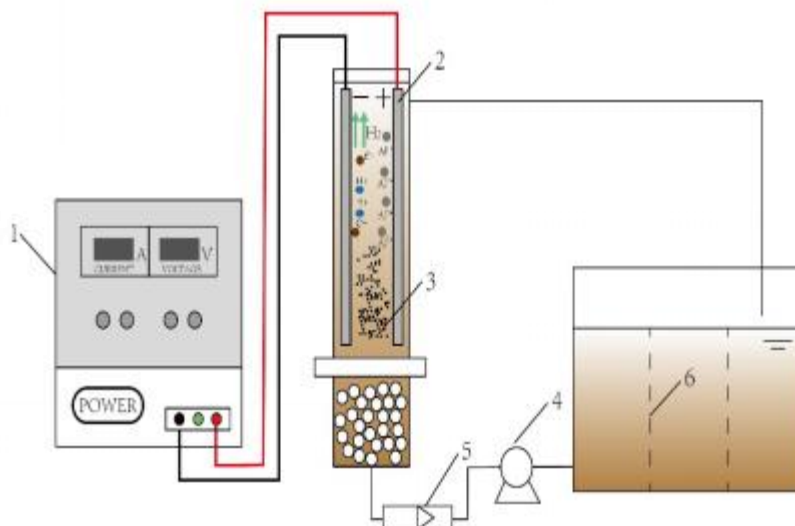
1-DC power, 2-Parallel Fe/Fe plates, 3-Granule electrode, 4-Pump, 5-Flowmeter, 6-Liquid storage tank

Figure 1. Three-dimensional electrocoagulation reactor

2.4. Cl⁻ removal tests

Approximately 2.4 g ZnAl-NO₃ LDH as the granule electrode was added between the Fe plates to treat 1.6 L desulfurization wastewater. The effective area of the plate electrode immersed in wastewater was 90 cm^2; 20-25 mL wastewater was sampled at 10 min intervals; the Cl⁻ concentration in the filtrate was determined by a Cl⁻-selective electrode; and the removal efficiency of Cl⁻ was calculated as follows:

$$\text{Removal efficiency} = \frac{C_0 - C_t}{C_t} \times 100\% \qquad (1)$$

where C_0 (mg/L) and C_t (mg/L) are the initial Cl⁻ concentration in raw water and the concentration at time (t), respectively.

3. RESULTS AND DISCUSSION

3.1. Characterization of ZnAl-NO₃ LDHs, MgAl-CO₃ LDHs and MgAl-CO₃ CLDHs

The XRD patterns of ZnAl-NO₃ LDHs, MgAl-CO₃ LDHs and MgAl-CO₃ CLDHs are shown in Fig. 2. The results show the characteristic diffraction of ZnAl-NO₃ LDHs and MgAl-CO₃ CLDHs before and after Cl⁻ adsorption. MgAl-CO₃ LDHs have no Cl⁻ adsorption effect, but only XRD characterization is used to reflect the structural change in MgAl-CO₃ LDHs after calcination, that is, the change to MgAl-CO₃ CLDHs.

The sharp and symmetrical diffraction peaks shown in Fig. 2(a) indicate good crystallization. The interplanar spacing of ZnAl-NO₃ LDHs is 8.91 Å, according to the calculation from the basic peak by the Bragg equation, and this value is similar to the reported literature [20], which indicates that NO₃⁻ was successfully intercalated into the layers of Zn-Al LDHs. As shown in Fig. 2(b), after Cl⁻ adsorption,

the interplanar spacing is increased from 8.91 Å to 11.10 Å, which indicates that the intercalated NO_3^- has been substituted by Cl^-, which is quite different, due to the adsorption ability of inorganic anions for LDH layers, generally following the order $CO_3^{2-}>SO_4^{2-}>OH^->F^->Cl^->Br^->NO_3^->I^-$ [21]. Theoretically, Cl^- can replace NO_3^- and can enter the LDH layer.
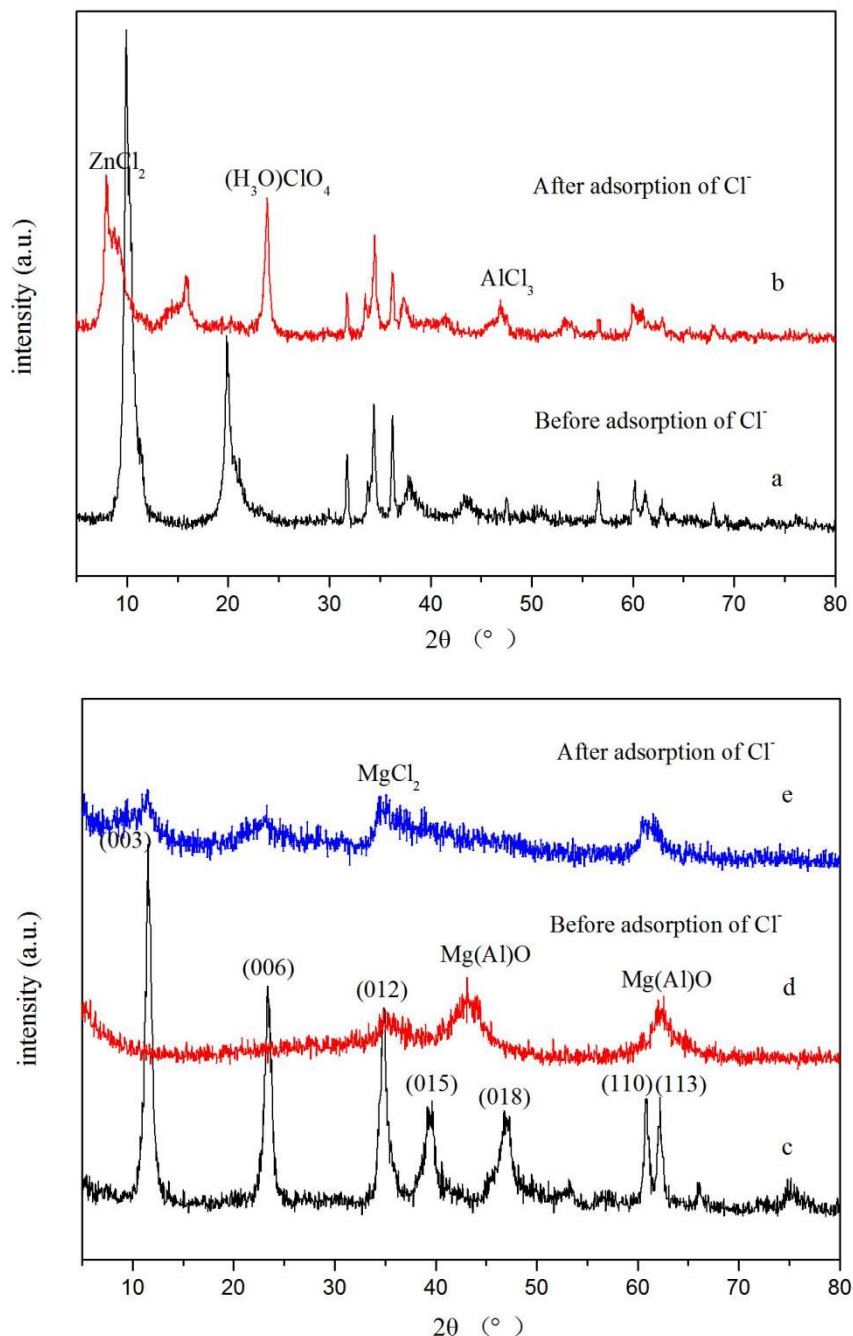
Figure 2. XRD patterns of ZnAl-NO_3^- LDHs before (a) and after adsorption of Cl^- (b); MgAl-CO_3 LDHs (c); and MgAl-CO_3 CLDHs before (d) and after (e) adsorption of Cl^-.

The diffraction peaks from the XRD pattern of MgAl-CO_3 LDHs (shown in Fig. 2(c)) were indexed to a hexagonal lattice with rhombohedral 3R symmetry. The basal peaks for the (003) plane indicate that the basal diffraction of carbonate ions entering the interlayer of Mg-Al LDHs can be obtained by using the Bragg equation [21]. Fig. 2(d) shows the pattern of MgAl-CO_3 CLDHs, the

calcined product of MgAl-CO₃ LDHs. The characteristic diffraction of the observed Mg(Al)O phase is ascribed to the collapsed layered structure after calcination, such that the loss of interlayer carbonate anions and water happens and amorphous mixed metal oxides are formed [22]. As shown in Fig. 2(e), after the adsorption of Cl⁻, the relative positions of the diffraction peaks are weakly symmetrical and broad; the calcined products of LDHs can be transformed into mixed metal oxides with a high specific surface area; the Cl⁻ in solution can be reabsorbed; and the layered structure can be partially restored [10].
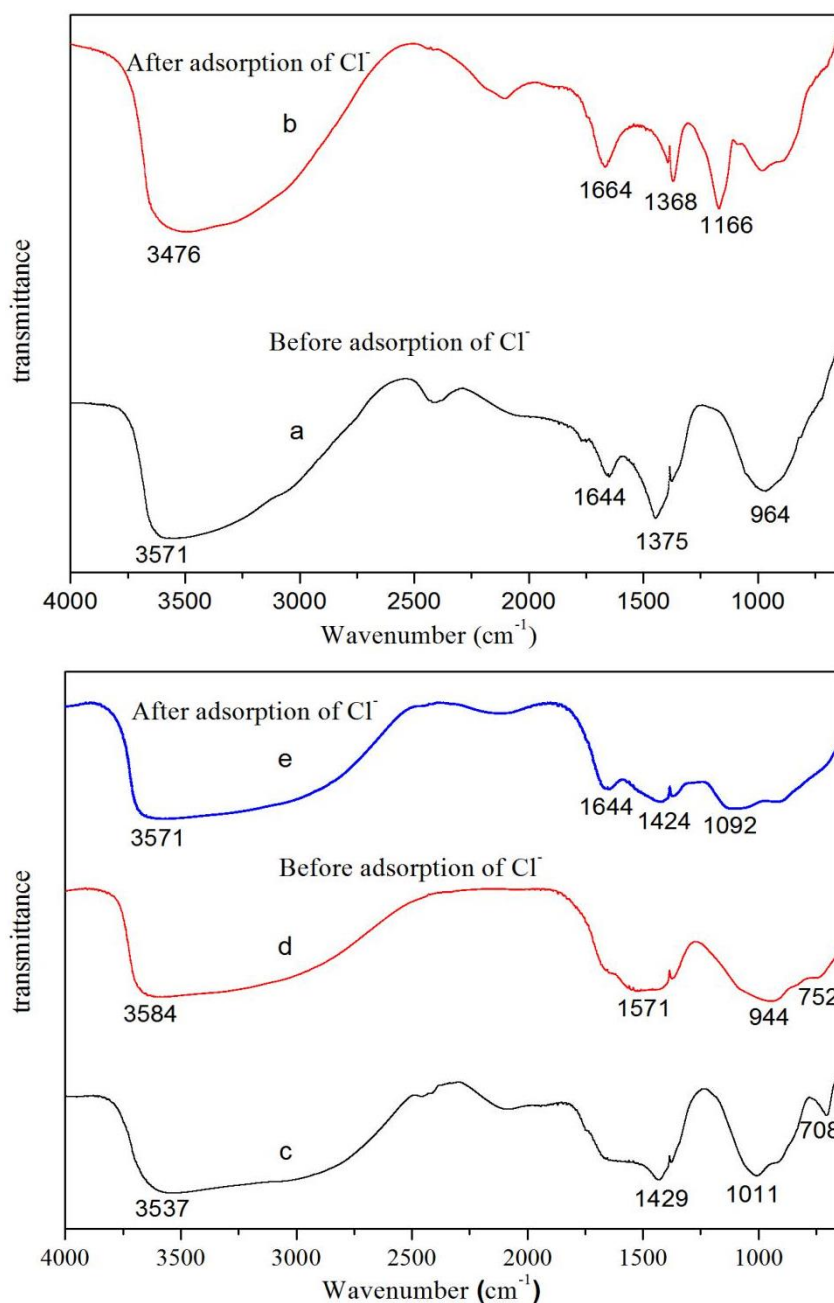

Figure 3. FTIR spectra of ZnAl-NO₃ LDHs before (a) and after adsorption of Cl⁻ (b); MgAl-CO₃ LDHs (c); MgAl-CO₃ CLDHs before (d) and after (e) adsorption of Cl⁻

The FTIR spectra of all synthesized LDH samples are shown in Fig. 3. The strong and broad band from 3600-3400 cm^{-1} is ascribed to the stretching vibration of O-H in the hydroxide layer and interlayer water [23]. The broad band at 1644 cm^{-1} is related to the bending vibration of H-O-H (δH_2O) of interlayer water molecules [24]. In Fig. 3(a), the small strong peak at approximately 1384 cm^{-1} is attributed to the antisymmetric stretching mode of the nitrate anions present in Zn-Al LDHs [25]. For the MgAl-CO$_3$ LDHs in Fig. 3(c), the band at 1429 cm^{-1} can be attributed to the antisymmetric stretching mode of carbonate. As seen in the FTIR spectra in Fig. 3(d), calcination partially destroys the crystal structure, consistent with the XRD pattern in Fig. 2(d), perhaps because of the partial loss of interlayer carbonate anions and water [26]. The band at 752 cm^{-1} present in the region from 400-800 cm^{-1} is attributed to the vibration modes of Mg-O, Al-O and Mg-O-Al in the LDH, as reported previously [24].
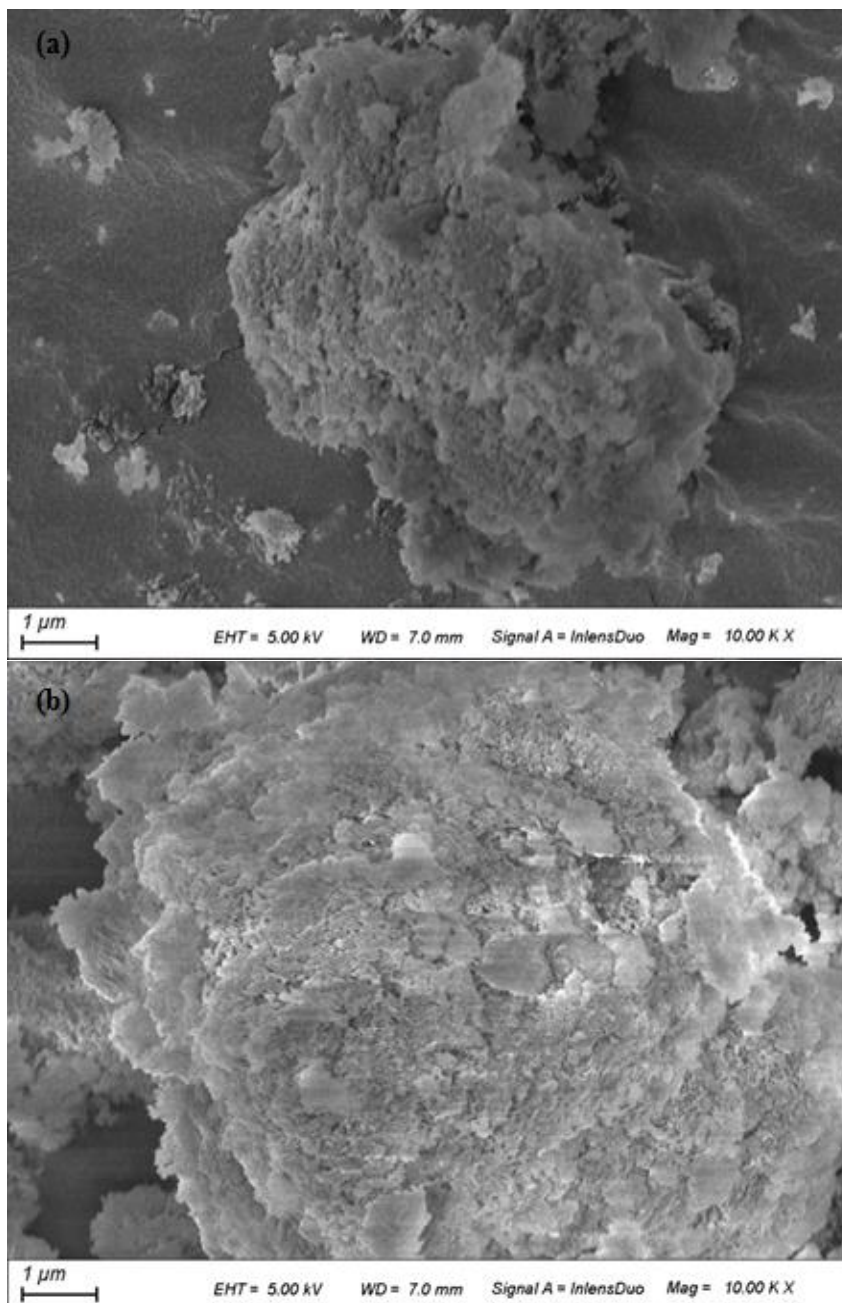
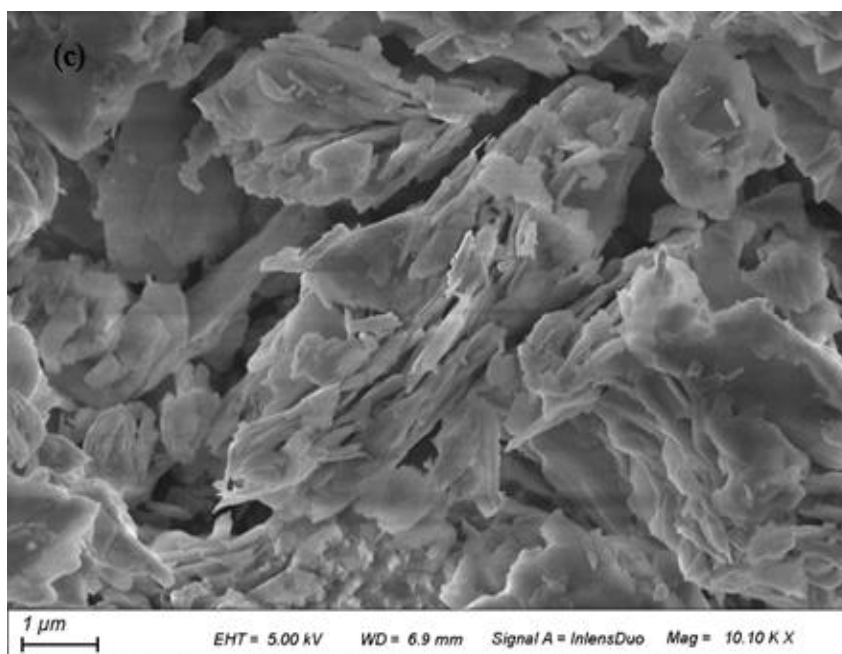**Figure 4.** SEM images of (a) ZnAl-NO₃ LDHs, (b) MgAl-CO₃ LDHs and (c) MgAl-CO₃ CLDHs

The bands at 1166 cm^{-1} in Fig. 3(b) and 1092 cm^{-1} in Fig. 3 (e) suggest that after the adsorption of Cl$^-$, Cl$^-$ enters the intercalated region of the Zn-Al LDH and Mg-Al LDH layers, respectively.

Fig. 4 shows the morphology of the ZnAl-NO₃ LDHs, MgAl-CO₃ LDHs and MgAl-CO₃ CLDHs. The slightly dark micrograph in Fig. 4 (a) shows that the material is composed of sheets that accumulate to form aggregates, and LDH sheets with partially slick surfaces are observed, which indicates the high crystallinity of ZnAl-NO₃ LDHs. As shown in Fig. 4 (b), the MgAl-CO₃ LDHs have a rough and bright surface. For the MgAl-CO₃ CLDH sample in Fig. 4 (c), calcination further reduces the granule size of the CLDH sheets, collapse of the layered structure occurs, and some irregular scattered sheet structures are formed [27].

TG and DSC are commonly used methods to characterize the thermal stability of LDHs. Fig. 5 shows the TG-DSC curves of MgAl-CO₃ LDHs, MgAl-CO₃ CLDHs and ZnAl-NO₃ LDHs. For MgAl-CO₃ LDHs (in Fig. 5 (a)), there are two weight loss stages: 10.93% from 24.47°C to 177.40°C and 25.99% from 170.40°C to 664.10°C. The first stage is attributed to the loss of interlayer and physisorbed water, while the second stage is due to the decomposition of interlayer carbonate and the release of hydroxyl ions from the layers [27]. The results are further proven by three different endothermic peaks at approximately 178.52°C, 227.56°C and 259.62°C in the corresponding DSC thermogram.

Similar to MgAl-CO₃ LDHs, two weight loss stages happen for MgAl-CO₃ CLDHs (shown in Fig. 5 (b)) in the range of 30.01-254.43°C and 254.43-675.52°C that correspond to a weight loss of 19.20% and 26.45%. The first mass loss is not obvious and is due to the adsorbed interlayer water [28]. The second stage of weight loss represents the further decomposition of interlayer carbonate [22], with an endothermic peak appearing at approximately 214.51°C.

Fig. 5 (c) shows the weight loss in the case of ZnAl-NO₃ LDHs. There were two weight losses at 29.74-208.21°C and 208.21-633.86°C, and the first weight loss interval (15.05%) was attributed principally to hydration and physisorbed water. The second weight loss (23.39%) was ascribed to the

decomposition of interlayer nitrates and dehydroxylation of the layers in the range of 208.21-633.86℃. The DSC thermogram shows two distinct endothermic peaks at 200.07℃ and 386.35℃, which are caused by the partial loss of ·OH from the hydroxide layer and decomposition reactions [29].
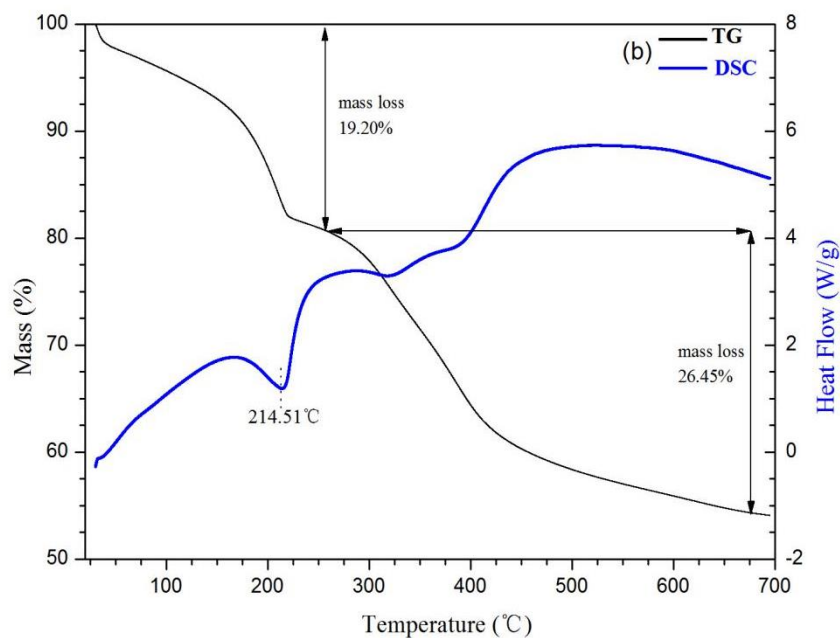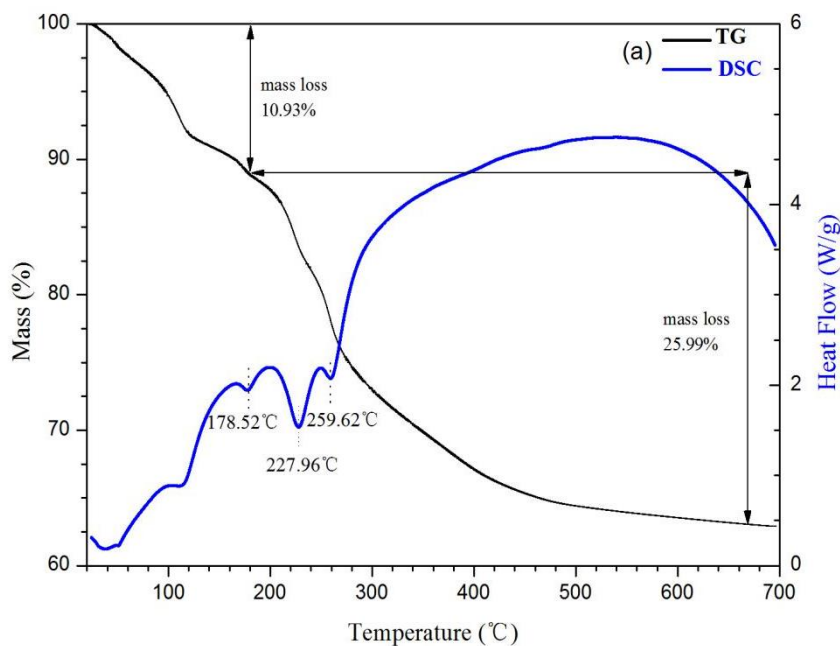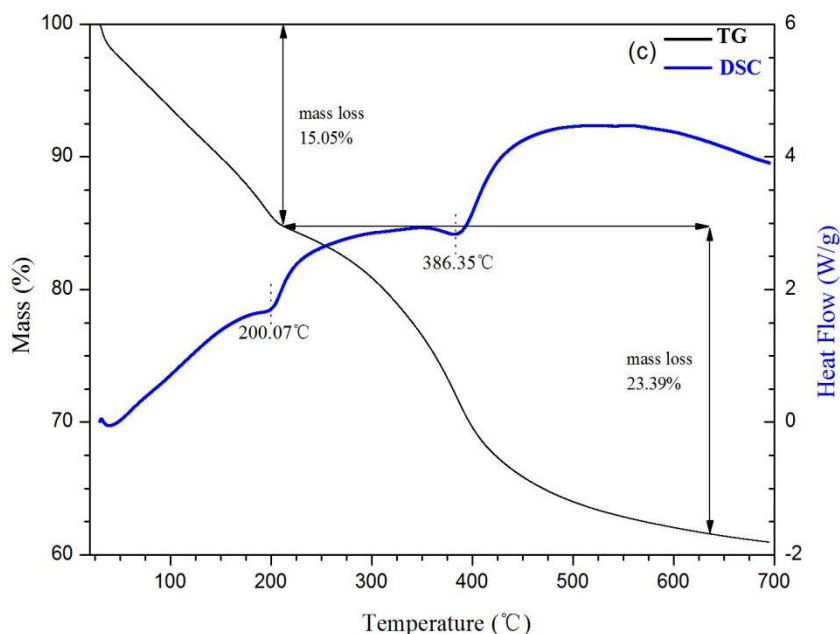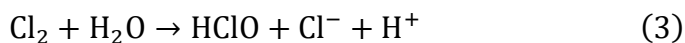
Figure 5. TG-DSC curves of synthesized LDHs: ZnAl-NO$_3$ LDHs (a), MgAl-CO$_3$ LDHs (b), and MgAl-CO$_3$ CLDHs (c)

3.2. Effect of current density on Cl$^-$ removal

As shown in Fig. 6 (a) and Fig. 6 (b), the optimal Cl$^-$ removal efficiency was 84.19% for ZnAl-NO$_3$ LDHs as the granule electrode and was obtained with an electrolysis time of 20 min and current density of 444 A/m^2. In the case of MgAl-CO$_3$ CLDHs, the maximum Cl$^-$ removal efficiency was 83.78% at a current density of 333 A/m^2. However, with increasing electrolysis time and current density, the removal efficiency of Cl$^-$ gradually decreased. Cl$^-$ could be removed efficiently at a lower current density. For chlorine-containing wastewater, the following reactions accompany the process of electrocoagulation [30]:

$$Cl^- \rightarrow Cl_2 + 2e^- \qquad\qquad (2)$$
$$Cl_2 + H_2O \rightarrow HClO + Cl^- + H^+ \qquad\qquad (3)$$
$$HClO \rightarrow ClO^- + H^+ \qquad\qquad (4)$$

The discharge potential of Cl$^-$ is 1.2 V (versus SCE). When the anode potential is higher than 1.2 V, Cl$^-$ oxidation occurs as reaction (2). During electrocoagulation, reactions (3) and (4) will then happen, and some gaseous chlorine escapes from the electrocoagulation reactor and is then dissolved in solution [31].
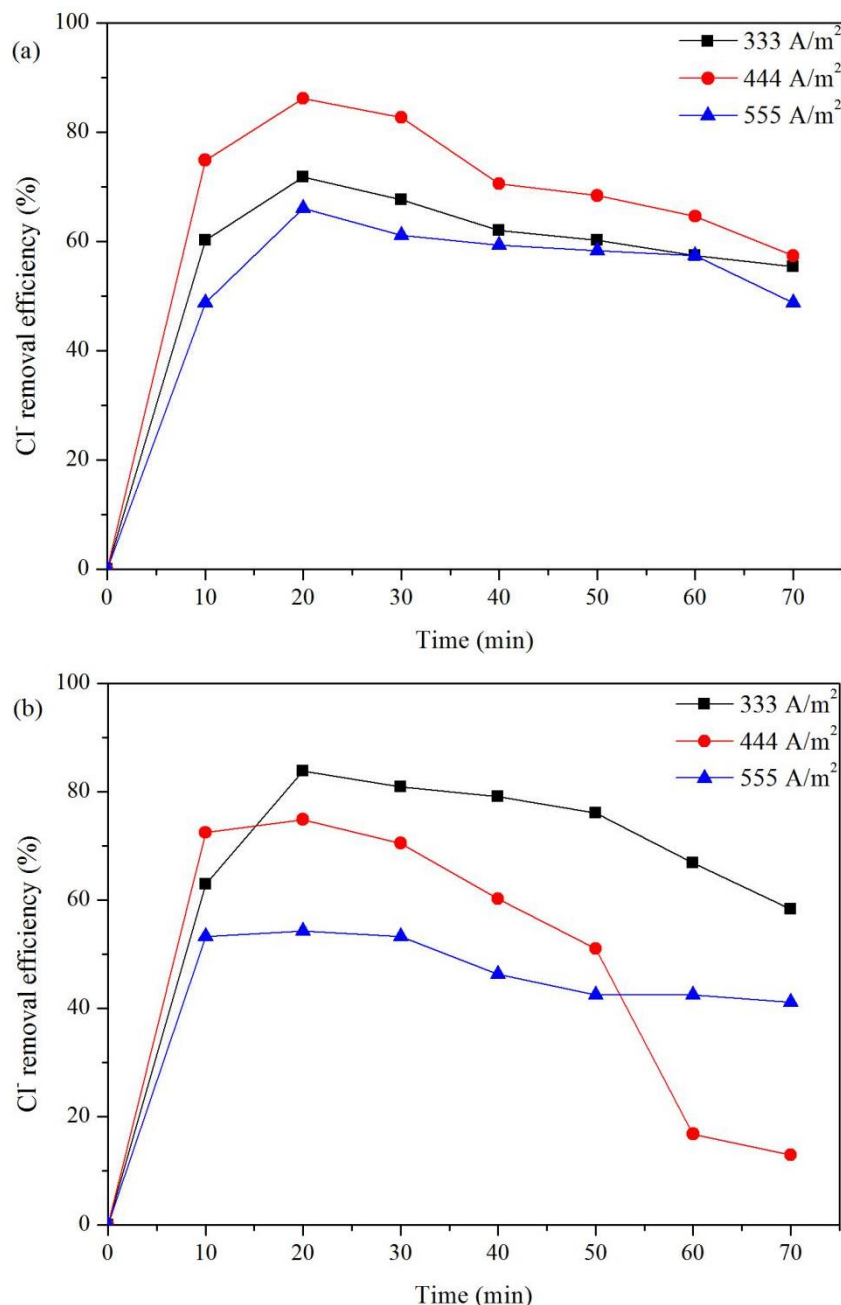
Figure 6. (a) Effect of current density on the removal of Cl⁻ by using ZnAl-NO₃ LDHs. (b) Effect of current density on the removal of Cl⁻ by using MgAl-CO₃ CLDHs.

3.3. Effect of electrode spacing on Cl⁻ removal

The space between electrodes directly affects the voltage drop, energy consumption and pollutant removal efficiency. When ZnAl-NO₃ LDHs are used as the granule electrode, the current density is constant at 444 A/m². When MgAl-CO₃ CLDHs are used as the granule electrode, the current density is constant at 333 A/m². The removal efficiency of Cl⁻ with different electrode spacings and electrolysis times is shown in Fig. 7 (a) and (b). When the electrode spacing is 1 cm, the removal efficiency of Cl⁻ is significantly higher than that at 2 cm. In Fig. 7 (a), as the electrolysis time increases from 10 to 20 min, the removal efficiency of Cl⁻ increases from 74.87% to 84.19%. According to Fig. 7(b), the removal efficiency of Cl⁻ increases from 62.86% to 83.78% as the electrolysis time increases from 10 to 20 min.

However, the removal efficiency of Cl^- decreases gradually as the electrolysis time increases. In the process of electrolysis, the thickness of the double layer formed becomes greater with smaller electrode spacing, and the distance from charged ions to the double layer becomes shorter. The movement resistance of ions in solution was reduced with smaller electrode spacing, thus improving the processing efficiency [32].
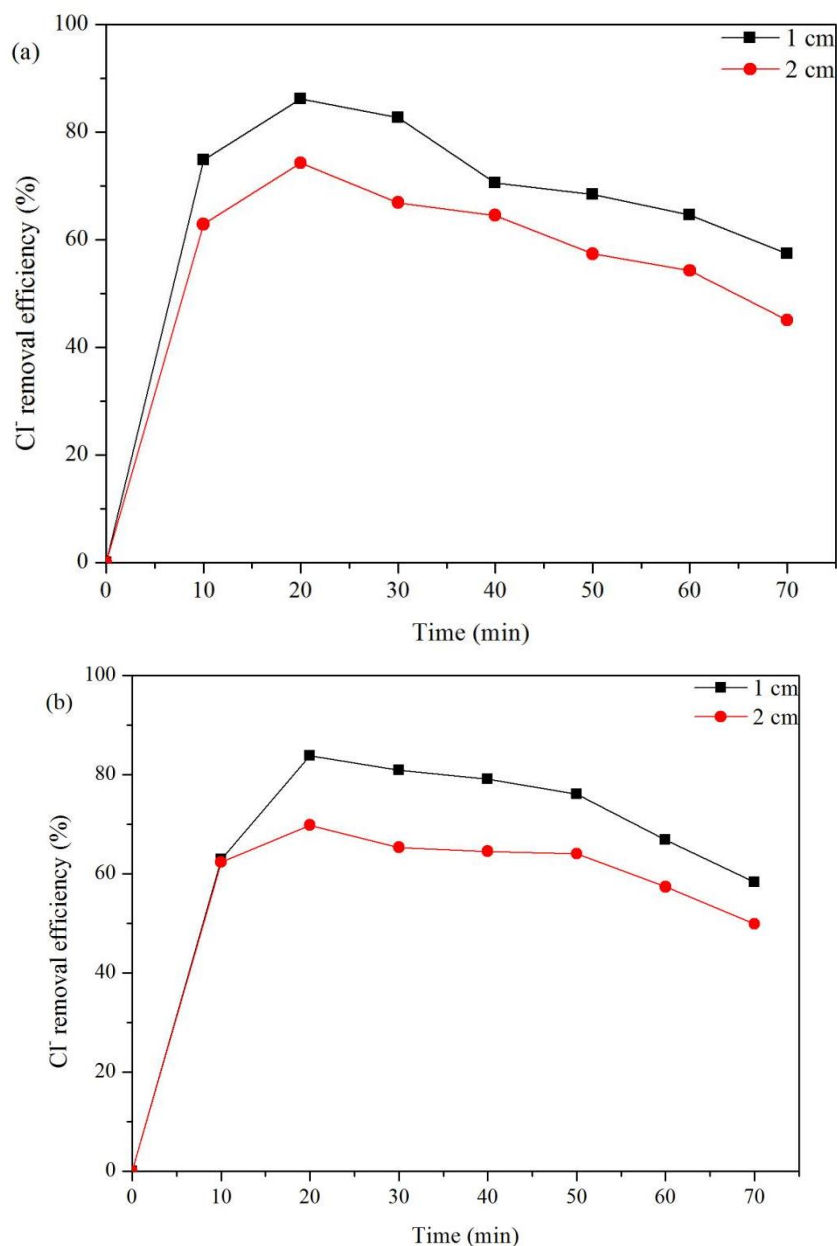

Figure 7. (a) Effect of electrode spacing on the removal of Cl^- by using ZnAl-NO_3 LDHs. (b) Effect of electrode spacing on the removal of Cl^- by using MgAl-CO_3 CLDHs.

3.4 Comparison of Cl⁻ removal efficiency from wastewaters via similar methods/materials

Table 1 lists some technologies used to treat Cl^--containing wastewater. According to Table 1, CLDH has good removal of Cl^-. CLDH can be used as a basis for treating desulfurization wastewater

with high chlorine concentrations. The three-dimensional electrochemical process shows better performance in Cl^- removal than the traditional two-dimensional electrochemical process.

Table 1. Technologies for Cl^- removal from wastewaters

Materials or technologies	Types of wastewater	Electrodes	Conditions	Removal of Cl^- (%)	References
CLDH adsorption (Mg–Al oxide)	sodium carbonate manufacturing wastewater		T=60°C, within 30 min, $1.5Mg_{0.80}Al_{0.20}O_{1.10}$	>90	[18]
EC (two-dimensional electrochemical process)	car wash wastewater	2 anodes/ 2cathodes: Fe/Al	Fe electrode: pH: 8, current density: 3 mA/cm², operating time: 30 min	Fe electrode: 50	[33]
			Al electrode: pH: 6, current density: 1 mA/cm², operating time: 30 min	Al electrode: 33	
Three-dimensional electrochemical process	petroleum refinery wastewater	Anode: graphite Cathode: graphite Granule electrode: Fe	Voltage: 12 V, Electrolyte dosage: 3 g/300 ml, Air flow: 1.5 L/min, Fe particle dosage: 4 g/300 ml, pH: 2.98	72.63	[34]
Three-dimensional electrochemical process (This work)	WFGD wastewater	Anode: Fe Cathode: Fe Granule electrode: LDH compounds	Granule electrode dosage: 1.5 g/L, $ZnAl-NO_3$ LDH: current density: 444 A/m², electrode spacing: 1cm, $MgAl-CO_3$ CLDHs: current density: 333 A/m², electrode spacing: 1cm	$ZnAl-NO_3$ LDH: 84.19 $MgAl-CO_3$ CLDHs: 83.78	

4. CONCLUSION

The anion adsorption ability of LDHs was proved by XRD and FTIR characterization. The three-dimensional electrocoagulation process has a remarkable effect on Cl^- removal from desulfurization wastewater. Considering the treatment cost and efficiency, the optimal reaction time was typically 20-30 min. At an electrode spacing of 1 cm and current density of 444 A/m², when $ZnAl-NO_3$ LDHs were used as the granule electrode, the removal efficiency of Cl^- was 84.19%. When $MgAl-CO_3$ CLDHs were

used as the granule electrode, the removal efficiency of Cl^- reached 83.78% under 1 cm electrode spacing and 444 A/m^2 current density.

References

1. Desulfurization and Denitration Committee of CAEPI, *China Environ. Prot. Ind.*, 7 (2018) 10.
2. P. Córdoba, *Fuel*, 144 (2015) 274.
3. B. Hu, Y. Yang, C. M. Yang, L. N. Zhang and L. J. Yang, *RSC Adv.*, 6 (2016) 113703.
4. X. Zhang, C. S. Ye, K. W. Pi, J. W. Huang, M. Xia and A. R. Gerson, *Sep. Purif. Technol.*, 211 (2019) 330.
5. P. Fang, Z. J. Tang, X. B. Chen, J. H. Huang, Z. X. Tang and C. P. Cen, *J. Chem.*, 2018 (2018) 1.
6. S. C. Ma, J. Chai , K. Wu , Z. C. Wan, Y. J. Xiang, J. R. Zhang and Z. X. Fan. *J. Ind. Eng. Chem.*, 66 (2018) 311.
7. S. C. Ma, J. Chai, G. D. Chen, W. J. Yu and S. J. Zhu, *Renew Sust. Energ. Rev.*, 58 (2016) 1143.
8. L. Cui, G. P. Li, Y. Z. Li, B. Yang, L. Q. Zhang, Y. Dong and C. Y. Ma, *Chem. Eng. Res. Des.*, 123 (2017) 240.
9. S. X. Jiang, Y. N. Li and P. L. Bradley, *Sci. Total Environ.*, 595 (2017) 567.
10. D. B. Gingerich, E. Grol and M. S. Mauter, *Environ. Sci.: Water Res. Technol.*, 4 (2018) 909.
11. H. Y. Zhang, T. S. Shang, C. Zhou, Y. B. Xue, T. F. Liu and W. Y. Tan, *Int. J. Electrochem. Sci.*, 14 (2019) 3114.
12. D. T. Moussa, M. H. El-Naas, M. Nasser, Al-Marri. Mustafa and J. Mohammed, *Environ. Manage.*, 186 (2017) 24.
13. N. Chubar, R. Gilmour, V. Gerda, M. Mičušík, M. Omastova, K. Heister, P. Man, J. Fraissard and V. Zaitsev, *Adv. Collioid Interface.*, 245 (2017) 62.
14. M. Q. Zhao, Q. Zhang, J. Q. Huang and F. Wei, *Adv. Funct. Mater.*, 22 (2012) 675.
15. Q. Wang and D. O'Hare, *Chem. Rev.*, 112 (2012) 4124.
16. R. Z. Ma, Z. P. Liu, L. Li, N. Iyi and T. Sasaki, *J. Mater. Chem.*, 16 (2006) 3809.
17. Z. X. Yang, H. Fischer and R. Polder, *Cem. Concr. Compos.*, 47 (2014) 87.
18. R. Hamidi and P. Kazemi, *Desalin. Water Treat.*, 54 (2015) 332.
19. T. Kameda, Y. Miyano, T. Yoshioka, M. Uchida and A. Okuwaki, *Chem. Lett.*, 29 (2000) 1136.
20. Y. Z. Chen, Z. G. Shui, W. Chen and G.W. Chen, *Constr. Build Mater.*, 93 (2015) 1051.
21. L. Lv, P. D. Sun, Z. Y. Gu, H. G. Dub, X. J. Panga, X. H. Taoa, R. F. Xua and L.L. Xua, *J. Hazard. Mater.*, 161 (2009) 1444.
22. M. A. Teixeira, A. B. Mageste, A. Dias, L.S. Virtuoso and K.P.F, *J. Cleaner Prod.*, 171 (2018) 275.
23. Y. J. Lin, Q. L. Fang and B. L. Chen, *J. Environ. Sci.*, 26 (2014) 493.
24. H. S. Ji, W. H. Wu, F. H. Li, X. X. Yu, J. J. Fu and L. Y. Jia, *J. Hazard. Mater.*, 334 (2017) 212.
25. F. Z. Mahjoubi, A. Khalidi, M. Abdennouri and N. Barka, *J. Taibah Univ. Sci.*, 11 (2017) 90.
26. F. R. Costa, A. Leuteritz, U.o Wagenknecht, D. Jehnichen, L. Häußler and G. Heinrich, *Appl. Clay. Sci.*, 38 (2008) 153.
27. A. A. A. Ahmed, Z. A. Talib, M. Z. B. Hussein and A. Zakaria, *J. Solid State Chem.*, 191 (2012) 271.
28. A. Elhalil, S. Qourzal, F. Z. Mahjoubi, R. Elmoubarki, M. Farnane, H. Tounsadi, M. Sadiq, M. Abdennouri and N. Barka, *Emerging Contam.*, 2 (2016) 42.

29. J. Xu, Y. Song, Q. Tan and L. H. Jiang, *J. Mater. Sci.*, 52 (2017) 5908.
30. S. Garcia-Segura, M. M. S. G. Eiband, J. V. de. Melo and C. A. Martínez-Huitle, *J. Electroanal. Chem.*, 801 (2017) 267.
31. Z. Sun, L. Chai, M. Liu, Y. D. Shu, Q. Z. Li, Y. Y. Wang, Q. W. Wang and D. F. Qiu, *Sep. Purif. Technol.*, 191 (2018) 424.
32. M. Yoosefian, S. Ahmadzadeh, M. Aghasi and M. Dolatabadi, *J. Mol. Liq.*, 225 (2017) 544.
33. Z. B. Gonder, G. Balcioglu, I. Vergil and Y. Kaya, *J. Environ. Manage.*, 2017 (200) 380.
34. L. Yan, Y. Wang, J. Li, H. Ma, H. Liu, T. Li and Y. Zhang, *Desalination*, 2014 (341) 87.